Symmetry of magnetoconductance fluctuations of quantum dots in the nonlinear response regime

A. Löfgren,[1,*] C. A. Marlow,[2] T. E. Humphrey,[3] I. Shorubalko,[4] R. P. Taylor,[2] P. Omling,[1] R. Newbury,[3] P. E. Lindelof,[5] and H. Linke[2,†]

[1]*Division of Solid State Physics and the Nanometer Structure Consortium, Lund University, SE-221 00 Lund, Sweden*

[2]*Materials Science Institute and Physics Department, University of Oregon, Eugene, Oregon 97403-1274, USA*

[3]*School of Physics, University of New South Wales, Sydney 2052, Australia*

[4]*HPFE6, ETH Zürich, CH-8093 Zürich, Switzerland*

[5]*Niels-Bohr Institute, University of Copenhagen, Universitetsparken 5, DK-2100 Copenhagen, Denmark*

(Received 26 October 2005; revised manuscript received 20 April 2006; published 12 June 2006)

We investigate the symmetry of magnetoconductance fluctuations of phase-coherent, two-terminal quantum dots in the nonlinear regime of transport. Specifically, we consider open, ballistic quantum dots (electron billiards) with and without symmetry axes parallel and perpendicular to the current direction and formulate a set of novel symmetry relations not observed in devices with lower symmetry. We experimentally confirm these relations, demonstrating that high-quality materials and modern semiconductor technology allow the fabrication of devices with almost perfect symmetry. Small deviations from the intended symmetry, presumably due to impurities and fabrication limitations, do exist and can be detected. We also take into account circuit-induced asymmetries of the measured conductance due to bias-dependent depletion and demonstrate that this effect can be experimentally distinguished from rectification effects that are due to a lack of device symmetry. Some open questions regarding the role of a magnetic field in the nonlinear regime of transport are highlighted.

DOI: 10.1103/PhysRevB.73.235321 PACS number(s): 73.40.Ei, 73.23.Ad, 73.50.Fq, 73.63.Kv

I. INTRODUCTION

Modern fabrication techniques allow us to fabricate mesoscopic semiconductor devices with well-defined geometry. In the ballistic transport regime, where the electron mean free path exceeds the device size, the device shape is known to have a significant influence on the transport properties.[1] In particular, the electronic properties of open quantum dots—that is, ballistic electron cavities in the phase-coherent transport regime—are explained in terms of the dot geometry.[2–7] However, while most previous studies were concerned with the linear response regime of transport much less attention has been paid to the nonlinear regime of transport and even less to the effect of magnetic fields in the nonlinear regime.

In the nonlinear regime of transport, electric conductance is—by definition—a function of the applied source-drain bias voltage. If the system is spatially asymmetric, the nonlinear conductance is in general not symmetric with respect to zero bias voltage. A net current is then generated by an ac-bias voltage, even when the bias is zero on time average. Such a rectification effect can, for instance, be observed in nature where the microscopically broken symmetry of certain crystals leads to the so-called photogalvanic effect.[8] A related effect has recently been demonstrated in artificial, ballistic antidot structures with designed asymmetry[9–12] and was demonstrated to be potentially useful for room-temperature, high-frequency applications.[13,14]

In the phase-coherent regime of transport, where conductance fluctuations due to wave interference are observed, nonlinear rectification was first observed in disordered, mesoscopic conductors in which symmetry was absent due to the random distribution of impurities.[15–19] Taylor *et al.* used for the first time ballistic cavities with intentionally high and low symmetry to experimentally establish reciprocity relations of magnetoconductance fluctuations in the linear response regime.[6,7] In more recent studies, we have investigated nonlinear rectification in intentionally asymmetric (triangular) quantum dots.[20,21] We found that the phase-coherent, nonlinear conductance was not symmetric because of the effect of an electric field on the wave interference inside the dot. Therefore, the observed nonsymmetry of the conductance is sensitively dependent on any parameter that shifts the electron phase, such as the amplitude of the applied bias, a small magnetic field, the device shape, or the Fermi energy. In these previous studies, we thus established the presence of rectification related to wave interference effects in devices lacking a symmetry axis with respect to the current direction.

Recently renewed interest in the symmetry of nonlinear conductance fluctuations focused on the role of magnetic field, in ballistic[22–26] and disordered[27] systems, including the high-magnetic-field regime.[28–30] Our own collaboration experimentally demonstrated the existence of magnetic-field asymmetries of the conductance in two-terminal quantum dots and established a set of symmetry relations for the nonlinear magnetoconductance in quantum dots with symmetry axes perpendicular and/or parallel to the current direction.[22]

Here, we expand on our previous results and report a more comprehensive investigation of these symmetry relations. Specifically, we investigate and compare devices fabricated from InP/InGaAs as well as GaAs/AlGaAs heterostructures, using both wet etching and surface gates, and we take into account bias-dependent depletion, both when formulating expected symmetry relations and in the analysis of experiments. We also use direct measurements of the net current to compare the degree of asymmetry in different devices.

We distinguish three sources of nonsymmetries in the nonlinear, phase-coherent conductance: first, the intentional

 ©2006 The American Physical Society

dot geometry—that is, the designed device symmetry with respect to the current direction. Second, we consider unintentional deviations from this geometry, such as small lithographic imperfections or impurities. Third, even a perfectly symmetric device may yield nonlinear rectification if placed in an asymmetric circuit. The origin of this effect is a bias-voltage-induced depletion gradient along the device. We demonstrate how this circuit-induced asymmetry can be distinguished experimentally from rectification due to the device shape.

The paper is structured as follows. In Sec. II we formulate a number of novel symmetry relations for the conductance in the nonlinear regime, with and without magnetic field, for quantum dots with symmetry axes parallel and perpendicular to the current direction. We distinguish between "nonrigid" devices, in which circuit-induced asymmetries of the conductance are significant, and "rigid" devices where this is not the case. Our devices and experimental techniques are described in Sec. III, and experimental results are presented in Sec. IV. Experiments are carried out in the regime of magnetic fields $B \gg \Phi_0/A$, where $\Phi_0 = h/e$ is the magnetic flux quantum and A is the device area, and for bias voltages larger than the characteristic energy scale (typically in the order of 10 μeV in open quantum dots). Magnetoconductance fluctuations obtained from devices that are not notably sensitive to circuit-induced asymmetries convincingly confirm all predicted symmetry relations and demonstrate that quantum dots can be fabricated with almost perfect symmetry. Averaging over many conductance fluctuations, which allows a quantitative comparison of the rectification observed in different devices, is carried out efficiently by direct measurement of the net current. We apply this technique to devices that are subject to circuit-induced asymmetries and show that this effect can be separated from rectification due to the actual device symmetry. We also study the asymmetry of triangular cavities as a function of magnetic field, which leads us to highlight, in Sec. V, some open questions regarding the role of a magnetic field in the nonlinear regime of transport.

II. CONDUCTANCE SYMMETRIES AS A FUNCTION OF DEVICE SYMMETRY

A. Basic symmetry relations

The linear response regime is defined by a conductance G, which does not depend on the applied source-drain voltage (denoted V and, from now on, referred to as the bias voltage). Regardless of the device symmetry, the current is then symmetric in voltage—that is, $I(V) = -I(-V)$. In the nonlinear regime, when the bias voltage is larger than the energy scale on which the device conductance varies,[31] G varies with the bias voltage. In the general nonlinear case, where a device has no microscopic symmetry (as is the case in a small disordered conductor), the phase-coherent conductance is not symmetric with respect to zero bias voltage, $G(V) \neq G(-V)$.[15–21,32–34] Such a device acts as a rectifier, and an average net current $I_{net} = 0.5[I(V_0) + I(-V_0)]$ is generated when a square wave of amplitude V_0 is applied to the device.

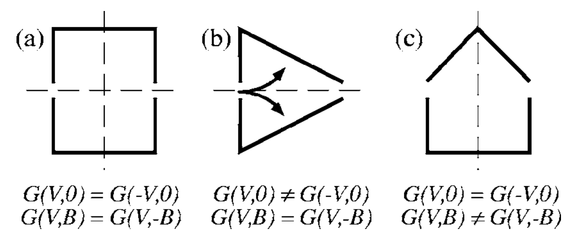

FIG. 1. Symmetry of $G(V,B)$ in rigid devices with (a) both UD (up-down) and LR (left-right) symmetry, (b) UD symmetry, but no LR symmetry, and (c) LR symmetry, but no UD symmetry.

Consider, however, a ballistic device that has a symmetry axis perpendicular to the current direction [Figs. 1(a) and 1(c)]. We refer to such devices as *left-right* (LR) symmetric. A perfectly LR-symmetric device, placed into a symmetric experimental setup, does not generate any net current, because it is affected in exactly the same way by a positive and a negative bias voltage [cf. Fig. 2(a)]. Hence the nonlinear conductance is symmetric with respect to zero bias voltage: $G(V) = G(-V)$.

Let us now consider the effect of a magnetic field B, perpendicular to the device plane. In linear response, the four-terminal resistance obeys the reciprocity relation $R_{12,34}(B) = R_{34,12}(-B)$.[35,36] Here, $R_{12,34}$ is the four-terminal resistance measured in a configuration where the current flows from contact 1 to 2 and the voltage drop is measured between contacts 3 and 4. In the following we limit ourselves to two-terminal devices and will discuss the conductance, which is the quantity measured in the experiments, rather than the resistance. For the special case of two-terminal devices, the reciprocity relation yields $G_{12}(B) = G_{12}(-B)$, where $G_{12}(B) = 1/R_{12,12}(B)$. Hence, the conductance is symmetric with respect to $B = 0$. This general result is true in the linear response regime, regardless of the device symmetry. In the nonlinear regime, this relation does not hold[1,31] and, in general, the two-terminal conductance is not symmetric in B:

$$G_{12}(V,B) \neq G_{12}(V,-B). \tag{1}$$

However, using simple symmetry arguments we can see that the symmetry in B still holds for devices with a symmetry axis parallel to the current[20]—so-called *up-down-* (UD-) symmetric devices [Figs. 1(a) and 1(b)]. The symmetry of the electrical potential implies conductance symmetry in B:

$$G_{12}(V,B) = G_{12}(V,-B). \tag{2}$$

This fundamental symmetry argument can be illustrated by considering classical electron trajectories [see Fig. 1(b)], the interference of which, in a semiclassical interpretation, leads to magnetoconductance fluctuations. In this picture, the electrons entering the dot from one side bend upwards for positive magnetic field and downwards for negative field.[22] If the device is perfectly UD symmetric, the trajectories will simply be mirrored about the horizontal axis and the transmission probability will be the same in both cases. As will be shown below, this symmetry relation is useful for experimental tests of the UD symmetry of a device.

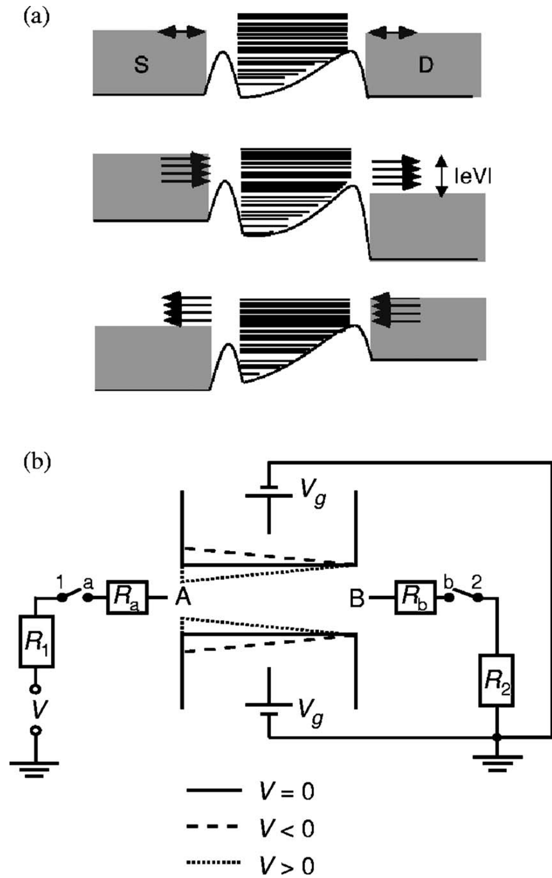

FIG. 2. Illustration of the origin of nonsymmetry in V of a quantum dot's nonlinear conductance. (a) Electron transport across a quantum dot without LR symmetry. The shape of the conductance band edge inside the dot illustrates the effect of spatial confinement inside the dot. The horizontal lines inside the dot indicate the modulation of the density of states due to overlapping, broadened single-electron states. Shading indicates the energy distribution functions in the electron reservoirs forming the source (S) and drain (D). *Top*: for very small voltages (linear response) the transmission probability (the conductance) is independent of the absolute value and the sign of the voltage. *Center and bottom*: illustration of the nonlinear response regime, where the potential and the electron states depend on the applied voltage. When the potential is not inversion symmetric, the electrical current flows via different sets of electronic states for positive and negative voltage, and rectification is observed (Ref. 20) (b). The effect of circuit asymmetry on a LR-symmetric channel. A bias voltage leads to a variation of the electrochemical potential along the channel. Consequently the depletion due to the gates and, therefore, the channel width vary along the channel. If the drain is used as the reference point of the gate voltage, the effective width varies more at the source side than at the drain side. A positive and a negative bias voltage alters the channel in different ways, resulting in a nonsymmetric nonlinear conductance. In our setup we use switches to reverse the circuit orientation. Forward grounding configuration $[G^{12}(V)]$ denotes that 1 is connected to a and 2 to b; in reverse configuration $[G^{21}(V)]$, 1 is connected to b and 2 to a. Symmetry relations of $G^{12}(V)$ and $G^{21}(V)$ for nonrigid devices (see Table I) apply only when serial resistances (including ohmic contacts and instrument impedances) are balanced such that $R_a = R_b$ and $R_1 = R_2$.

In the context of the semiclassical argument used in the preceding paragraph, it is important to note that the symmetry arguments presented throughout this paper are fundamental and do not make any assumptions about the actual physical mechanism that causes the nonlinear terms of the conductance. For instance, a finite contribution of electron-electron interaction to this nonlinearity, as considered in Refs. 27 and 23 for $B < \Phi_0/A$ and bias smaller than the Thouless energy, requires the same spatial scattering or capacitive asymmetry as illustrated in Fig. 1(c)[23]

B. Symmetry relations in the presence of circuit-induced asymmetry

Strictly speaking, LR symmetry requires the entire experimental setup to be perfectly symmetric with respect to the device's LR symmetry axis. One common reason for why a particular setup may not be symmetric is the choice of reference point of the voltage applied to the gates that form the device. Usually the gate voltage is defined with respect to the drain reservoir, located at one side of the device, as illustrated in Fig. 2(b). In linear response, when only negligible bias voltages are used, this circuit asymmetry is of no consequence. When appreciable bias voltages are used, however, the resulting gradient in local electrochemical potential along the device will deform the device potential in a way that depends on the voltage sign [see Fig. 2(b)]. Consequently a nonsymmetric conductance will be measured: $G(V) \neq G(-V)$.[37–39]

We will refer to this effect as *circuit-induced asymmetry* (CIA). Specifically, we will use this expression to describe any nonlinear behavior for which the grounding point of the gates relative to source and drain is important. In the definition of this term we include any asymmetric nonlinear behavior observed in ideal, perfectly LR symmetric devices, but we do not include rectification related solely to the intentional or unintentional asymmetry of the actual device.

In the following, we will discuss how circuit-induced asymmetry in a LR-symmetric device can be experimentally distinguished from rectification due to the actual device shape. To do so, we measure the device in both forward and reverse directions by interchanging the connections of the source and drain contacts. In particular, using a switch, we physically swap the source and drain connections, while keeping the drain contact as the reference point of the gate voltage [see Fig. 2(b)].[40] We let $G^{12}(V)$ denote the conductance with the device in the forward grounding configuration. $G^{21}(V)$ denotes the conductance with the device in the reversed configuration [Fig. 2(b)]. CIA is expected to be significant only when the bias-induced potential gradient along the device is comparable to the change in gate voltage (V_g) required to cause an appreciable change in depletion—that is, when $\partial G/\partial V \approx \partial G/\partial V_g$.[39] A device for which $\partial G/\partial V_g \ll \partial G/\partial V$ (no CIA is observed) will be referred to as *rigid*, while a device in which CIA is observed will be referred to as *nonrigid*. Symmetry relations for rigid and nonrigid devices with and without LR symmetry will now be presented.

1. Zero magnetic field

a. A rigid device with LR symmetry. A rigid, LR-symmetric device is affected in the same way by a positive

and a negative bias voltage and the nonlinear conductance is symmetric around zero bias voltage: $G^{12}(V)=G^{12}(-V)$. Because of the symmetry of the device and because it is rigid, the reversal of source and drain will not change the conductance: $G^{12}(V)=G^{21}(V)$.

b. A rigid device without LR symmetry. Next, let us consider a rigid device lacking LR symmetry. The nonlinear conductance is changed if we either reverse source and drain or change the sign of the applied bias. However, if we change the sign of the applied bias and reverse source and drain, the same conductance is obtained. This observation leads to the following relations:

$$G^{12}(V) \neq G^{12}(-V) \tag{3}$$

and

$$G^{12}(V) = G^{21}(-V). \tag{4}$$

It follows from Eq. (4) that the antisymmetric part of the conductance, $G^A(V)=0.5[G^{12}(V)-G^{12}(-V)]$, can also be obtained by taking the difference of the conductance of the device in the two grounding configurations:

$$G^{12}(V) - G^{21}(V) = 2G^A(V). \tag{5}$$

$G^A(V)$ determines the net current observed when an ac voltage is applied to the device.

c. A nonrigid device with LR symmetry. For a nonrigid LR-symmetric device, the circuit asymmetry yields a nonsymmetric nonlinear conductance

$$G^{12}(V) \neq G^{12}(-V). \tag{6}$$

However, reversing the grounding arrangement, in an otherwise perfectly symmetric experimental setup (that is, $R_1 = R_2$ and $R_a = R_b$ in Fig. 2), will not change the conductance and we expect

$$G^{12}(V) = G^{21}(V). \tag{7}$$

and

$$G^{12}(V) - G^{21}(-V) = 2G^A(V). \tag{8}$$

As we will show later, the difference between relations (5) and (8) can be used to experimentally distinguish between circuit-induced asymmetric nonlinear behavior in a LR symmetric, nonrigid device and that caused by the absence of LR symmetry in a rigid device.

d. A nonrigid device without LR symmetry. The situation is more complicated for a nonrigid device without LR symmetry. In this case, there is no simple symmetry relation. Thus, we have chosen to consider the conductance as consisting of parts with different symmetry relations. The antisymmetric part of the conductance will contain one part that is reversed when the grounding configuration is reversed [$G_r(V)$, just as in a rigid device], one part that is unchanged [$G_{CIA}(V)$, as expected for a nonrigid, LR symmetric device], and one part with no special relation. The total conductance can then be expressed as $G(V)=G_r(V)+G_{CIA}(V)+G_x(V)$, where G_r fulfills relations (3)–(5), G_{CIA} obeys relations

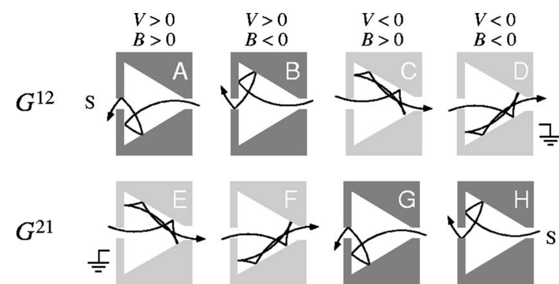

FIG. 3. Illustration, using classical electron orbits, of the symmetry relations for a rigid device in the nonlinear regime and in finite magnetic fields. The upper row shows the device in forward grounding configuration and the lower row in reversed configuration, where the source is indicated by S and the location of the drain is indicated by a grounding sign. A positive magnetic field is taken to be into the page. A positive bias voltage in forward configuration injects electrons through the right-hand opening. The difference in gray shade illustrates that the potential of the device differs for positive and negative voltages [see also Fig. 2(a)], which means that the device potential (and therefore the transmission probability) differs between, for instance, (A) and (D) in the nonlinear regime (illustrated by different orbits). Note that, e.g., (A) and (B) give the same orbits if the device is UD symmetric [$G^{12}(V,B)=G^{12}(V,-B)$, Eq. (2)], but not if the device is lacking UD symmetry. However, independent of the device shape of a rigid device, e.g., (A) and (G) always give the same orbits and the same transmission probability, $G^{12}(V,B)=G^{21}(-V,B)$ [see Eq. (10)].

(6)–(8), and G_x is an additional term with no specific relation between G_x^{12} and G_x^{21}. By subtracting $G^{21}(V)$ from $G^{12}(V)$ we obtain

$$G^{12}(V) - G^{21}(V) = 2G_r^A(V) + 0 + G_x^{12}(V) - G_x^{21}(V). \tag{9}$$

Significantly, G_{CIA} has, by intention, disappeared—that is, we have succeeded in removing the asymmetric part of the nonlinear conductance originating from the circuit asymmetry in a LR symmetric device. The remaining terms in Eq. (9) are all related to the asymmetry of the device, and any contribution to the antisymmetric conductance (and, thus, to rectification) that would be present also in a LR-symmetric device has been removed. The fact that the circuit asymmetry also generates a contribution to the nonlinear conductance that differs between measurements in the two grounding configurations, and is not subtracted, contributes to the conduction asymmetry in a device lacking LR symmetry.

2. Magnetic field

In zero magnetic field, a rigid device of arbitrary shape fulfills Eq. (4). In nonzero magnetic fields, this equation becomes

$$G^{12}(V,B) = G^{21}(-V,B). \tag{10}$$

This relation is illustrated in Fig. 3 [compare, for instance, (A) and (G) or (C) and (E)].

If the rigid device is LR symmetric, the simpler relation

TABLE I. A summary of the symmetry relations valid in the nonlinear regime for rigid and non rigid devices of different spatial symmetry.

	UD, not LR	LR, not UD	Arbitrary shape
Rigid	$G(V,B)=G(V,-B)$ $G(V,B)\neq G(-V,-B)$ $G^{12}(V,B)=G^{21}(-V,B)$	$G(V,B)\neq G(V,-B)$ $G(V,B)=G(-V,-B)$ $G^{12}(V,B)=G^{21}(-V,B)$	$G^{12}(V,B)=G^{21}(-V,B)$
Nonrigid	$G(V,B)=G(V,-B)$	$G(V,B)\neq G(-V,-B)$ $G^{12}(V,B)=G^{21}(V,-B)$	

$$G^{12}(V,B) = G^{12}(-V,-B) \tag{11}$$

is fulfilled. This relation holds regardless of the UD symmetry of a device. Note that it is important to keep track of the sign of B in finite magnetic field.

For a nonrigid device there is no simple relation between the bottom and top rows of Fig. 3, and no general relation exists for a device of arbitrary shape. However, for a nonrigid, LR symmetric device, Eq. (7) becomes, in finite magnetic fields,

$$G^{12}(V,B) = G^{21}(V,-B). \tag{12}$$

Describing this in words, to obtain the same conductance upon reversal of the grounding configuration, one needs to change the direction of the magnetic field.

It should also be noted that a perfectly UD-symmetric device will be UD symmetric even if it is nonrigid. The applied bias changes the effective gate voltage along the current direction giving LR asymmetry, but it is changed by the same amount for the upper and lower gates and does not introduce any UD asymmetry in UD-symmetric devices. Thus, Eq. (2), $G^{12}(V,B)=G^{12}(V,-B)$, is fulfilled for both rigid and nonrigid, UD-symmetric devices, independent of whether they are LR symmetric or not.

Table I summarizes the symmetry relations (1) and (12).

C. Differential conductance

So far we have discussed the symmetry relations for the conductance, defined as $G=I/V$. However, in experiments usually the differential conductance $g=\partial I/\partial V$ is measured.

We will now show that the differential conductance obeys the same symmetry relations as the conductance. Let us start by showing that if $G(V,B)$ is symmetric in V, then also $g(V,B)$ is symmetric in V. We expand

$$G(V,B) = \sum_n c_{2n}(B)V^{2n}, \tag{13}$$

where all coefficients c_n are independent of V and all the odd terms equal zero as a result of the assumed symmetry in V. This yields

$$I(V,B) = G(V,B)V = \sum_n c_{2n}(B)V^{2n+1} \tag{14}$$

and

$$g(V,B) = \frac{\partial I(V,B)}{\partial V} = \sum_n c_{2n}(B)(2n+1)V^{2n}. \tag{15}$$

Hence, the differential conductance $g(V,B)$ is symmetric in V if G is symmetric in V.

Similarly, by expanding G in B, it can be shown that $g(V,B)$ is symmetric in B if $G(V,B)$ is symmetric in B. Also, it follows that if the conductance is antisymmetric in V or B, the differential conductance is antisymmetric as well. It can be concluded that the differential conductance fulfills the symmetry relations derived for the conductance in Sec. II B.

D. Comparing the degree of asymmetry

We are interested in quantifying the degree of asymmetry of the nonlinear conductance in quantum dots with different intentional symmetries. The simplest way to do this is to directly measure the dot's differential conductance as a function of B or V. This approach is employed in Sec. IV A and allows for effective verification of expected symmetry relations for a specific device.

A more advanced approach is useful if we want to compare the amount of nonsymmetry present in two different devices. As the nonsymmetric nonlinear conductance in our asymmetric devices is due to quantum interference effects,[20,21] the asymmetry will differ as a function of Fermi energy and magnetic field. Hence, if we compare the degree of asymmetry for different devices, statistics for at least one of these parameters are needed in order to quantify the asymmetry induced by the devices.

A convenient way of obtaining statistics about LR symmetry is to measure the net current

$$\begin{aligned} I_{net} &= 0.5[I(V_0) + I(-V_0)] \\ &= 0.5\left[\int_0^{V_0} g(V)dV + \int_0^{-V_0} g(V)dV\right] \\ &= 0.5\int_0^{V_0} dV[g(V) - g(-V)] \end{aligned} \tag{16}$$

generated by a square-wave voltage signal of amplitude V_0, referred to as the rocking amplitude. This is the antisymmetric part of the differential conductance summed up over the voltage range $[0,\pm V_0]$. Thus, the net current directly provides us with a measure of the degree of asymmetry in V of the nonlinear conductance. To be able to quantitatively com-

TABLE II. A summary of the devices discussed in the text. All triangular devices used are equilateral with sidelength s.

Device	Shape	Symmetries	Size (μm)	T (K)	Material	Confinement	Top gate
$T1$	Triangle	UD	$s=2.0$	0.3	GaAs/AlGaAs	Etched	Yes
R	Rectangle	UD, LR	1.7×2.0	0.3	GaAs/AlGaAs	Etched	Yes
$T2$	Triangle	UD	$s=2.6$	0.03	GaAs/AlGaAs	Split gate	No
C			1.6×10	0.03	GaAs/AlGaAs	Split gate	No
$T3$	Triangle	UD	$s=1.0$	0.3	InP/InGaAs	Etched	Yes
$T4$	Triangle	LR	$s=1.0$	0.3	InP/InGaAs	Etched	Yes

pare the asymmetry generated by different rocking amplitudes V_0, we define the normalized net current N by

$$N(V_0)=\frac{I_{net}}{V_0}=\frac{0.5}{V_0}\int_0^{V_0}dV[g(V)-g(-V)]. \quad (17)$$

The normalized net current can be measured directly as a function of Fermi energy or magnetic field. Measuring N as a function of one parameter, such as the magnetic field, thus corresponds to averaging over bias voltage and magnetic field, in a single measurement—a highly efficient measurement method.

In order to distinguish between devices with and without LR symmetry, we define $N^{LR}=0.5(N^{12}-N^{21})$. From Eqs. (17) and (9) we obtain

$$\begin{aligned}N^{LR}(V_0)&=0.5[N^{12}(V_0)-N^{21}(V_0)]\\&=\frac{0.5}{V_0}\int_0^{V_0}dV[g_r^A(V)-g_r^A(-V)+0+\Delta g_x(V)]\\&=N_r(V_0)+\Delta N_x(V_0),\end{aligned} \quad (18)$$

where $\Delta g_x(V)=0.5[g_x^{12}(V)-g_x^{12}(-V)-g_x^{21}(V)+g_x^{21}(-V)]$. Here, $\Delta g_x(V)$ and $\Delta N_x(V)$ represent the contribution to the nonlinear conductance without symmetry relations. Note that CIA of a LR symmetric device does not contribute to N^{LR}.

In the presence of a magnetic field we define

$$\begin{aligned}N^{LR}(V_0,B)&=0.5[N^{12}(V_0,B)-N^{21}(V_0,-B)]\\&=\frac{0.5}{V_0}\int_0^{V_0}dV[\Delta g_r(V,B)+0+\Delta g_x(V,B)],\end{aligned} \quad (19)$$

where $\Delta g_r^{12}(V,B)=g_r^{12}(V,B)-g_r^{12}(-V,B)-g_r^{21}(V,-B)-g_r^{21}(-V,-B)$. Any CIA in a LR-symmetric device is subtracted and does not contribute to $N^{LR}(V_0,B)$. $N^{LR}(V_0,B)$ will be used to compare the degree of asymmetry induced by devices with and without LR symmetry. The *magnitude* of N^{LR} will give a measure of the asymmetry of the nonlinear conductance.

We will also use the normalized net current to investigate whether the devices are UD symmetric with respect to the induced asymmetry of the nonlinear conductance. This technique does require some lack of LR symmetry in the device so that a net current is obtained. In Sec. II B we noticed that circuit asymmetry will not introduce any UD asymmetry in a perfectly UD-symmetric sample. Hence, we will use N^{12} to investigate the devices with respect to UD symmetry. From Eqs. (2) and (17) it follows that also the normalized net current will be symmetric in B for a UD-symmetric device. It is the degree of *symmetry in B* of N^{12} which tells us about the degree of UD symmetry of the device.

III. EXPERIMENTAL DETAILS

A. Devices

The devices used in this work were fabricated from modulation-doped GaAs/AlGaAs heterostructures and InP/GaInAs heterostructures, using electron-beam lithography followed by either wet etching or metal evaporation to produce split gates. We show results from six different quantum dots: four equilateral triangles (denoted $T1$, $T2$, $T3$, and $T4$), one rectangle (denoted R), and one structure with neither UD nor LR symmetry (denoted C). An overview of the device parameters is given in Table II, and the device geometries are shown in Fig. 4.

Triangle $T1$ and rectangle R were fabricated from modulation-doped GaAs/AlGaAs material. The two-dimensional electron gas (2DEG) was located 90 nm below the surface and had a carrier density of 2.5×10^{15} m^{-2} and a mobility of 125 m^2/(V s). These devices were defined by shallow wet etching. They were covered with a top gate, which was separated from the device surface by an approximately 1-μm resist layer and which was used to change the Fermi energy. $T1$ was equilateral (sidelength $s=2$ μm) with one contact opening in the middle of the base and the other

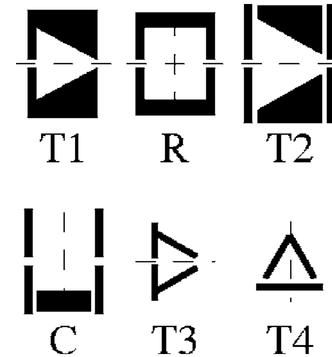

FIG. 4. Illustration of the device geometries. See text and Table II for details.

one in the opposite corner, as shown in Fig. 4. R had a width of 1.7 μm and a height of 2.0 μm, and the contact openings were positioned symmetrically as shown in Fig. 1. For these devices, $\partial g/\partial V_g \approx 3\ (e^2/h)/\text{V}$.

Triangle $T2$ and device C were fabricated from modulation-doped GaAs/AlGaAs material with the 2DEG located 80 nm below the surface, with a carrier density of $2.1\times 10^{15}\ \text{m}^{-2}$ and a mobility of $70\ \text{m}^2/(\text{V s})$. They were defined with split gates. Six gates were used to define the triangle: one pair to form each of the two quantum point contacts (QPC's) and one pair defining the central part of the triangle ($s=2.6\ \mu$m; cf. Fig. 4). Device C was an open structure defined by five gates: two pairs defining the QPC's separated by a distance of 1.6 μm and the fifth rectangular gate defining a wall parallel to the current axis, positioned 0.8 μm below the QPC's. There was no gate opposite to the fifth gate; hence, the width of this structure was given by the mesa—i.e., approximately 10 μm. This structure was not UD symmetric. In general, different gate voltages were applied to the two QPC's and the device was not LR symmetric. For these devices, $\partial g/\partial V_g \approx 20\ (e^2/h)/\text{V}$.

The triangular dots $T3$ and $T4$ were fabricated from modulation-doped InGaAs/InP material,[41,42] with the 9-nm-thick quantum well located 40 nm below the surface. The carrier density was $7.7\times 10^{15}\ \text{m}^{-2}$ and the mobility was $45\ \text{m}^2/(\text{V s})$. We expect CIA to be important when the variation of the conductance with gate voltage is comparable to other nonlinear effects—that is, when $\partial g/\partial V_g \approx \partial g/\partial V$. Because the InP/InGaAs devices were defined by deep wet etching rather than by surface gates and because a Ti/Au top gate used to tune the carrier concentration was separated from the quantum well by a 1-μm layer of insulating polymer, $\partial g/\partial V_g \approx 0.6\ (e^2/h)/\text{V}$ was one to two orders of magnitude smaller than in typical, surface-gated GaAs/AlGaAs devices. It may also be important that wet-etched InP/InGaAs dots have been found to have a substantially ohardero (steeper) confinement potential than GaAs/AlGaAs devices,[43] again reducing the sensistivity of the dot conductance to small changes in the gate voltage. Both $T3$ and $T4$ had side length 1.0 μm, but the contact openings were positioned such that $T3$ was UD symmetric and $T4$ was LR symmetric (see Fig. 4).

For all devices considered here the cross-sectional area is of order μm^2, such that the magnetic field corresponding to one flux quantum is of order mT. The Thouless energy for all devices is of order 10 μeV. The devices $T1$, R, $T3$, and $T4$ were measured at $T=0.3$ K in a ^{3}He cryostat at base temperature 230 mK. The split-gated devices $T2$ and C were measured in a dilution refrigerator with a base temperature of 30 mK.

B. Experimental methods

For measurements of the two-terminal conductance in the linear response regime, we used separate current and voltage probes in a four-point geometry, with an excitation voltage $eV_{ac} < k_B T$ (25 μeV at $T=300$ mK). The measurements of the differential conductance in nonlinear response were carried out by adding a dc component to the small ac signal. For direct measurement of the net current,[34,44] we used a 191-Hz, symmetric square wave with amplitude V_0 (also referred to as the rocking amplitude), which was 100% amplitude modulated with a frequency of 17 Hz. This means that a square-wave bias was applied during half of the longer period and no bias was applied during the other half. The time-averaged net current was then detected using a lock-in amplifier, phase-locked to the slower modulation frequency. The modulation frequency was always kept above 10 Hz to avoid distortion of the applied wave, and the rocking frequency was kept below 1 kHz to avoid any high-frequency effects. Under these conditions the results were not sensitive to the chosen frequencies and the system could be considered to be in a steady state at all times, because the rocking frequency was slow compared to all electronic time scales. To observe symmetry relations, it is necessary to have a symmetric experimental setup, with equal voltage drops on each side of the device. To achieve this, all series resistances in the setup, including Ohmic contacts and the cryostat wiring, were measured and compensated to be symmetric with respect to the device [see Fig. 2(b)]. We also verified that there were no other rectifying contributions, such as imperfect Ohmic contacts. Finally, we also checked that no net current was obtained if we replaced the device with an Ohmic resistor for test purposes. The drain reservoir was used as the reference point of the split gates and the top gates. All values for source-drain bias voltages given in the following refer to the voltage drop over the device itself.

Note that in principle it is possible to minimize CIA effects in surface-gated devices by using as a reference point for the gate voltage a point that is kept at a potential halfway between the source and drain, using a voltage divider.[44,45] However, the present work aimed at establishing symmetry relations in the presence of CIA effects and results obtained with minimized CIA are reported elsewhere.

IV. EXPERIMENTAL RESULTS AND DISCUSSION

A. Direct measurement of the symmetry relations

In this section, we will investigate the symmetry relations by direct conductance measurements for the InP/InGaAs triangles $T3$ and $T4$ (top gate voltage zero). We begin by establishing the behavior of the devices in the linear response regime. The upper curve in Fig. 5 shows magnetoconductance measurements in linear response for triangle $T4$. Quickly varying conductance fluctuations, due to electron wave interference, are overlaid on a slowly varying background, which can be related to classical commensurability effects.[5] The rms value of the conductance fluctuations is about $0.1e^2/h$, which is a typical value for quantum dots of similar size, measured at 0.3 K. The conductance fluctuations are of the same order of magnitude for all devices. Note that the conductance fluctuations are almost perfectly symmetric in B, as expected in the linear response regime where $G_{\alpha\beta}(B)=G_{\alpha\beta}(-B)$ (cf. Sec. II A).

Figure 6 shows the magnetoconductance measurements in the nonlinear response regime for the triangle $T3$, which is UD symmetric but not LR symmetric, for all configurations shown in Fig. 3, $V=\pm 0.8$ mV (1 mV over the whole circuit).

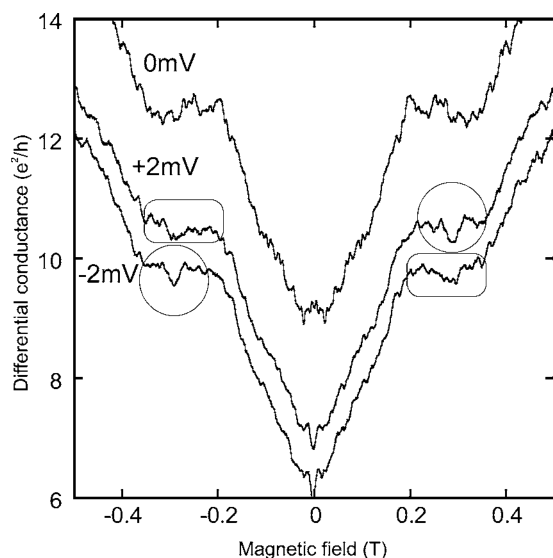

FIG. 5. Magnetoconductance of the LR-symmetric triangle $T4$. *Upper curve*: zero-bias and linear response regime. Note the almost perfect symmetry in B, which is expected for linear response. *Lower curves*: nonlinear response with $V=\pm 1.6$ mV. The symmetry in B is broken, which is evident by comparing the features inside the thin circles and rectangles at +0.3 T or −0.3 T. However, by comparing the features inside the two circles (or alternatively the rectangles) the symmetry relation $g(V,B)=g(-V,-B)$ [see Eq. (11)] becomes apparent.

The first thing to note, by comparing Fig. 6(a) with 6(b) and Fig. 6(c) with 6(d), is that the nonlinear conductance is nonsymmetric in V.

One can show that this nonsymmetry is not induced by the circuit, but by the absence of LR symmetry in the device. For a rigid device, the relation $G^{12}(V,B)=G^{21}(-V,B)$ [Eq. (10)] is upheld for any device of arbitrary shape. Significant CIA should, however, break this symmetry. Noting the strong similarity of, for instance, curves (B) and (E) in Fig. 6, it can be concluded that CIA is negligible compared to the effect of the intentional asymmetry in this particular device. In other words, this InP/InGaAs device is rigid.

For a perfectly UD-symmetric device, we expect that $g(V,B)=g(V,-B)$ regardless of the amount of CIA (see Table I). The graphs in Fig. 6 have been grouped such that each pair of graphs in each of the subfigures allows a check of this symmetry relation, for either positive or negative bias voltage and in either forward or reverse grounding configuration. Hence, comparing the two curves in the same graph gives a direct measure of the degree of UD symmetry. Overall the agreement between each pair is remarkably good, even though small deviations, not related to measurement noise, are apparent.

The deviations from expected symmetries caused by the effect of (i) the CIA, (ii) the deviations from UD symmetry, and (iii) the lack of LR symmetry are quantified in the inset of Fig. 6(a). This is done by integrating the absolute value of the difference between those curves that should be identical according to the relevant symmetry relations:

$$A(B) = \int_0^B dB\{|g^n_{diff}|\}. \tag{20}$$

Here, g_{diff} is given by (i) $g_{diff}=g^{12}(V,B)-g^{21}(-V,B)$, which in the absence of any measurement noise should equal zero for rigid devices of any shape, (ii) $g_{diff}=g(V,B)-g(V,-B)$, which should equal zero for perfectly UD-symmetric devices, and (iii) $g_{diff}=g(V,B)-g(-V,-B)$, which should equal zero for rigid, perfectly LR-symmetric devices. For each case (i)–(iii), the result of the integral is averaged for all four relevant combinations giving g_{diff} [e.g., A-F, B-E, C-H, and D-G for case (i)] and the average is shown in the inset. The result shows that the intentional deviation from LR symmetry causes the largest differences, the unintentional deviation from UD symmetry causes smaller deviations, and CIA causes the smallest deviations, confirming what is also apparent from direct observation.

In Fig. 5 we show magnetoconductance fluctuations measured in the nonlinear regime for the LR symmetric triangle $T4$, $V=1.6$ mV (2 mV over the whole circuit). Crucially, as expected for a device lacking UD symmetry, one finds that $G(V,B)\neq G(V,-B)$ for finite V. However, according to Eq. (11) we expect $g(V,B)=g(-V,-B)$ if CIA can be neglected. Indeed, the expected symmetry relation can be observed, for instance by comparing the marked features.

To summarize this section, we have shown, by direct magnetoconductance measurements on the triangles $T3$ and $T4$ fabricated from InP/InGaAs material, that we can recover all the symmetry relations expected from the intentional device symmetries for rigid devices. In particular, the symmetry in B for the UD-symmetric device indicates that the role of imperfections of the device geometry is small.

B. Net current measurements

We will now use net current measurements to investigate the symmetry of the GaAs/AlGaAs devices. Three points should be made. First, the measurement of a net current requires the presence of some LR asymmetry; otherwise, there would be no signal. Second, the net current measurements of the GaAs/AlGaAs devices show a significant CIA effect, because in these devices the conductance varied much faster with gate voltage than in the InP/InGaAs devices. Also, as we are only tracing the small part of the conductance being antisymmetric in V, it is much more sensitive to all kind of deviations, such as CIA or imperfections. Here, we will mainly present results for the triangles and, unless otherwise indicated, we show results from triangle $T1$. We begin by asking whether the triangles are UD symmetric, as measured by the net current fluctuations.

1. Basic results

In Fig. 7 we show measurements of the normalized net current as a function of magnetic field for both forward and reverse grounding configurations—that is, N^{12} and N^{21} [cf. Eq. (17)]. The rocking amplitude V_0 was 1 mV. The net current varies as a function of magnetic field, and both positive and negative net currents are obtained. The magnetic field

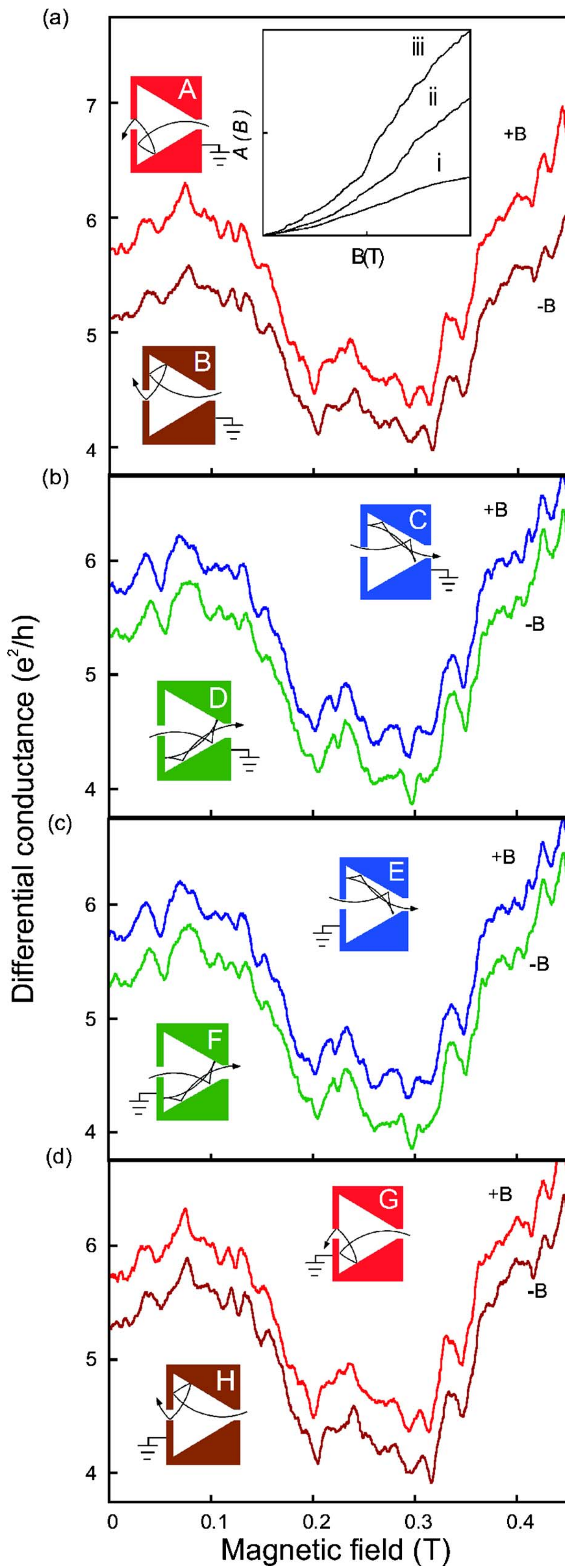

FIG. 6. (Color online) Magnetoconductance of the UD-symmetric triangle $T3$ in the nonlinear regime. Each figure shows graphs for positive and negative magnetic fields in different grounding configurations. (a) shows $g^{12}(+V,\pm B)$, (b) shows $g^{12}(-V,\pm B)$, (c) shows $g^{21}(+V,\pm B)$, and (d) shows $g^{21}(-V,\pm B)$ (V=0.8 mV). *Inset*: the quantified, normalized deviations $A(B)$ in arbitrary units [Eq. (20)] from the expected symmetry relations caused by (i) the CIA, (ii) the deviations from UD symmetry, and (iii) the lack of LR symmetry are shown here. $A(B)$ was integrated over the range 0–0.5 T.

scale of the current oscillations is similar to the scale of the conductance fluctuations, indicating that the main contribution to the rectification is due to quantum interference effects, as described in Ref. 20. We observe that there is a shift between the data obtained in the two grounding configurations, but qualitatively they are very similar. Basically all maxima and minima can be seen in both measurements. The small difference between N^{12} and N^{21} means that some CIA is present. However, in the following section we will focus on UD symmetry, which is not expected to be affected by

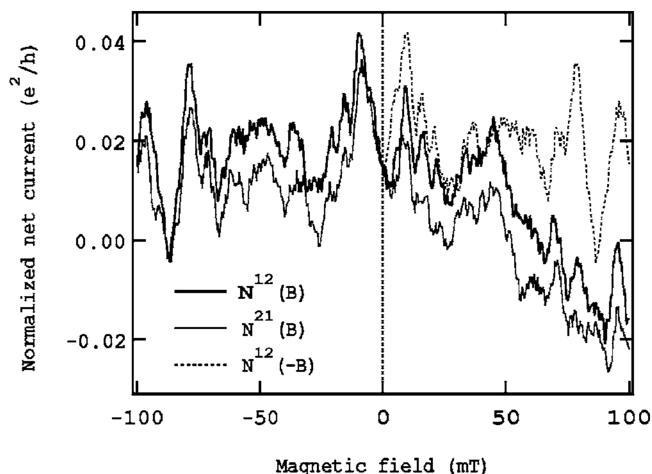

FIG. 7. Comparison of the normalized net current [cf. Eq. (17)] of the UD-symmetric triangle $T1$ measured with the device in forward grounding configuration (N^{12}, thick solid line) and reversed configuration (N^{21}, thin solid line), with a rocking amplitude of $V_0=1$ mV. The curves are not identical, but qualitatively very similar with maxima and minima at the same fields. Note that the net current is not symmetric with respect to zero magnetic field. The dotted line shows $N^{12}(B)$ mirrored around the $B=0$ axis—i.e., $N^{12}(-B)$—for a direct comparison of the asymmetry in B.

CIA, and we will limit ourselves to only show measurements for one grounding configuration. In Fig. 8 we show measurements of the normalized net current taken at different top gate voltages (Fermi energies). While all curves show oscillations of approximately the same amplitude and period, the oscillations are essentially uncorrelated for the different gate voltages. This observation is consistent with the origin of the fluctuations being quantum interference.

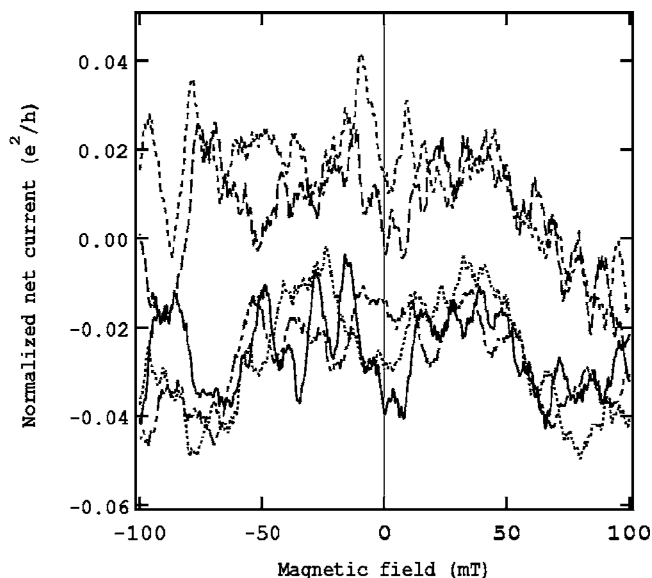

FIG. 8. Normalized net current N^{12} of triangle $T1$ as a function of magnetic field, where the different curves are measured at various gate voltages (Fermi energies). From top down at $B=0$, $V_g=-1.2, 0, -3.4, -2.7, -1.9$ V, corresponding to $\mu_F=7.9, 8.5, 6.8, 7.2, 7.6$ meV ($V_0=1$ mV).

2. UD symmetry

For a perfectly UD-symmetric device, the induced net current would be symmetric in B, as stated in Eq. (2). Some of the curves in Figs. 7 and 8 are relatively symmetric for small magnetic fields, while others are more or less antisymmetric. Neither of them are fully symmetric in the entire range shown. The dotted line in Fig. 7 shows the left half of $N^{12}(B)$ mirrored around the zero-magnetic-field axis. A comparison between the dotted line and $N^{12}(B)$ gives a direct visual comparison of $N^{12}(B)$ and $N^{12}(-B)$. They are not identical, but there is a clear correlation up to about 50 mT: the maxima and minima appear at approximately the same positive and negative fields. Another way of studying the symmetry in B is to divide the curves into their symmetric and antisymmetric parts, $N^S=0.5[N(B)+N(-B)]$ and $N^A=0.5[N(B)-N(-B)]$, respectively. This is done in Fig. 9, which shows the symmetric and antisymmetric parts of the measurements shown in Fig. 8. The antisymmetric part in B should equal zero for a perfectly UD-symmetric device (cf. last paragraph of Sec. II B). The finite values of the antisymmetric part of the net current in Fig. 9(b) indicate that the device is not fully UD symmetric.

In Fig. 10 we compare the symmetry in B for three different structures: the two nominally UD-symmetric triangles $T1$ and $T2$ and device C without UD symmetry. In order to generate a net current we use different split-gate voltages for the two QPC's of device C, breaking the LR symmetry of the device. We expect the net current of the UD-symmetric triangles to be symmetric in B, while there is no reason for the net current generated by device C to be symmetric in B. Neither of the curves is fully symmetric in B, but while there indeed is a correlation between $N(B)$ and $N(-B)$ for the triangles, for magnetic fields smaller than approximately 50 mT, there is no such correlation for device C.

We have also studied the asymmetry at various rocking amplitudes. Quantum interference effects are washed out at a bias exceeding a few mV, because of heating effects and because of phase breaking due to inelastic electron-electron scattering.[31,46–48] Thus, we expect that any net current persisting, or developing, at a high bias (rocking amplitude) must be of an origin other than wave interference. Figure 11 shows the symmetric and antisymmetric parts of the normalized net current for increasing rocking amplitude and for constant top gate voltage. The curves in Fig. 11(b) are vertically offset by $0.01e^2/h$, and the horizontal lines correspond to the zero lines for the different curves. The amplitude of the fast oscillations with a period of 10–20 mT decreases with increased bias voltage. At $V_0>2$ mV the net current oscillations have basically vanished, which is consistent with the fact that the fast magnetoconductance fluctuations are totally washed out at this rocking amplitude in this device. A large symmetric part evolves at high rocking amplitudes, and a smaller antisymmetric part remains as well. The gross features which remain at higher rocking amplitudes change slowly with gate voltage (Fermi energy) and are correlated for different Fermi energies (not shown here). As the triangle is not LR symmetric we expect that it exhibits asymmetric nonlinear behavior also when any quantum interference effects are washed out. This thermally averaged part is also

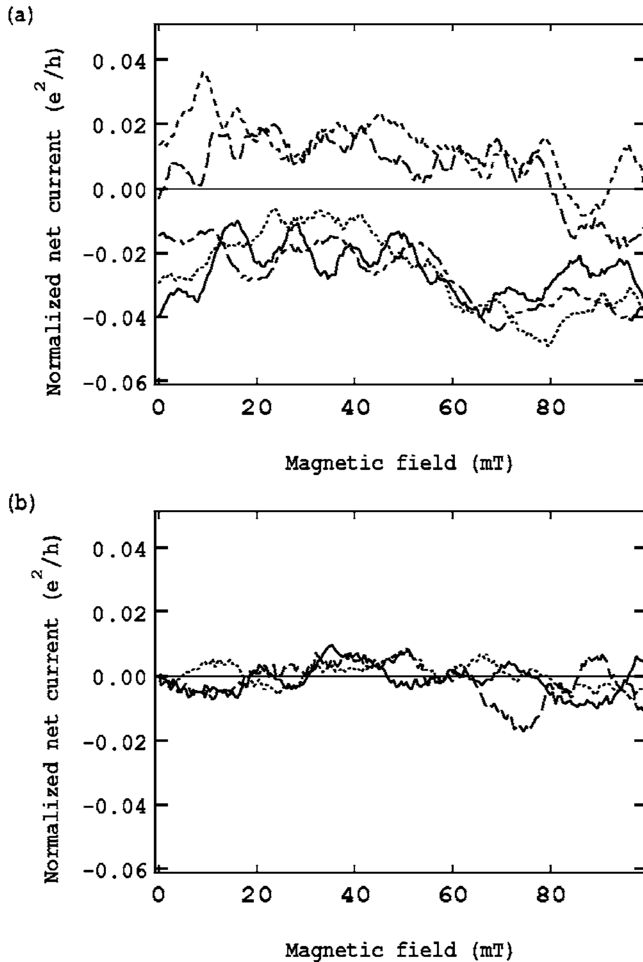

FIG. 9. Separation of the $N^{12}(B)$ curves of triangle $T1$ in Fig. 8, into contributions that are (a) symmetric N^S and (b) antisymmetric N^A with respect to $B=0$ ($V_0=1$ mV). Specifically, $N^S=0.5[N(B)+N(-B)]$ and $N^A=0.5[N(B)-N(-B)]$. For perfectly UD-symmetric devices one would expect the traces in (b) to be identical to zero. The finite values of the curves indicate that there is some UD asymmetry. The curves in (a) have finite values because of the (intended) LR asymmetry. Curves measured at the same top gate voltage are plotted with equal line type in both graphs of this figure and in Fig. 8.

likely to increase with increased bias voltage and should not depend as sensitively on the Fermi energy (top gate voltage). Hence, the observations are in agreement with our expectations.

C. Does an intentionally LR-symmetric device generate less net current than a device lacking LR symmetry?

It can be expected that an intentionally LR-symmetric device is not perfectly symmetric on a microscopic scale. Is an intentionally symmetric quantum dot, such as R, more symmetric than an intentionally asymmetric quantum dot, such as $T1$? We ask this question with respect to the induced asymmetry of the phase-coherent, nonlinear, conductance fluctuations. For the rigid devices shown in Sec. IV A, based on InP/InGaAs, the answer to this question is a clear "yes"

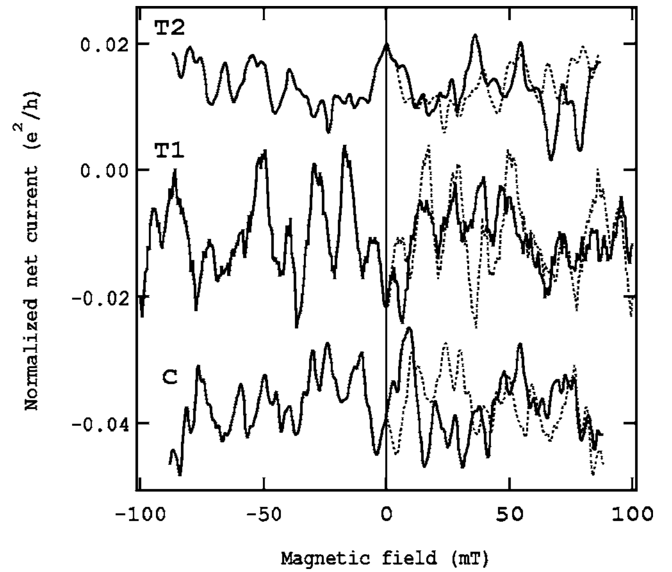

FIG. 10. Normalized net current N^{12} for three different devices as a function of B, with $V_0=0.5$ mV. The devices are the UD-symmetric split-gated triangle $T2$, the UD-symmetric wet-etched triangle $T1$, and the split-gated device C without UD symmetry. The curves are vertically offset for clarity. The dotted curves are mirrored around $B=0$. Thus, the right half of the graph gives a direct comparison between $N^{12}(B)$ and $N^{12}(-B)$.

(Figs. 5 and 6). Here we pose the question, is this true for devices fabricated from another, less rigid, material system (GaAs/AlGaAs) as well? In order to compare the degree of asymmetry of different devices, we need to average over Fermi energy or magnetic field for specific, fixed bias voltages.

To remove contributions to the asymmetric conductance that are due to CIA and that are not related to any broken LR symmetry of the device, we follow the procedure outlined in Eqs. (18) and (19) and determine the difference of net currents measured in the two configurations: $N^{LR}(V,B)=0.5[N^{12}(V,B)-N^{21}(V,-B)]$. After this treatment, we indeed still observe a nonzero net current, which then must be related to deviations from LR symmetry in the device. To obtain statistics allowing us to quantify the amount of LR symmetry in the devices, we average N^{LR} over a sufficiently large magnetic-field range. To choose a suitable range, we note in Fig. 11 that the period of the net current fluctuations changes at approximately 100 mT. Therefore, we have chosen to use $\sigma(N^{LR})$, the standard deviation of $N^{LR}(B)$, in the range $-100<B<+100$ mT, as a parameter. It is well known that the amount of quantum interference effects differs for various devices. For this reason, to quantify the asymmetry, we use $\sigma(N^{LR})/\sigma(\Delta G)$, which is the ratio of the standard deviation of the normalized net current and the standard deviation of the conductance fluctuations measured without bias. In Fig. 12, this ratio is plotted as a function of top gate voltage (Fermi energy). Clearly, we see that the induced asymmetry of the triangle is larger than for the rectangle. If we define the ratio r of the asymmetry induced by the triangle and the rectangle as

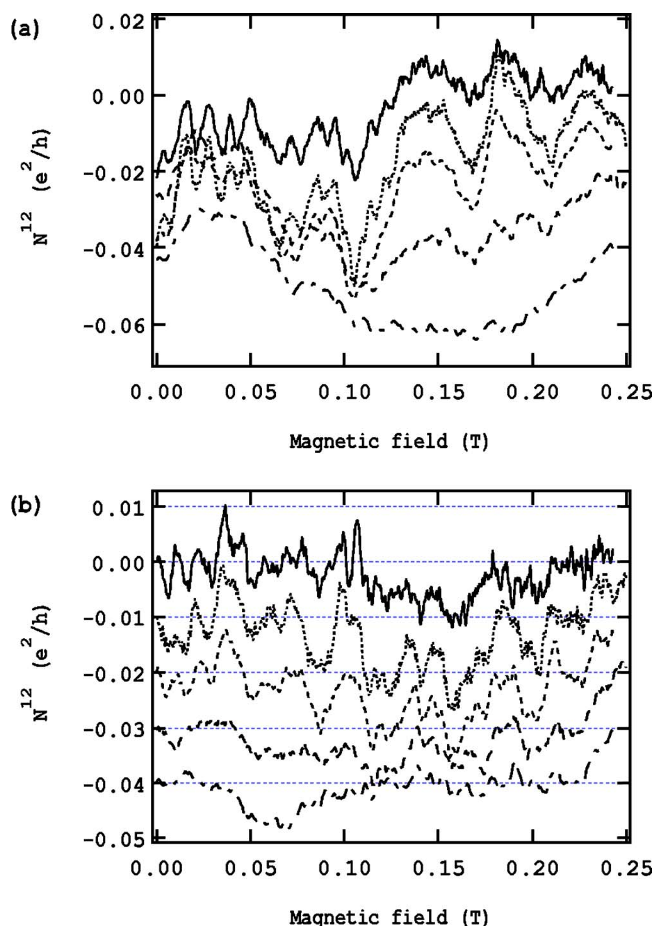

FIG. 11. (Color online) The (a) symmetric and (b) antisymmetric parts of the normalized net current N^{12} at different rocking amplitudes and constant top gate voltage for triangle $T1$ (V_g=−1.9 V, μ_F=7.6 meV). From top down the rocking amplitudes are 0.55 meV, 1.2 meV, 1.6 meV, 2.6 meV, and 3.6 meV. The curves in (b) are offset and are mutually separated by $0.01e^2/h$.

$$r = \frac{\sigma(N_{tri}^{LR})/\sigma(\Delta G_{tri})}{\sigma(N_{rect}^{LR})/\sigma(\Delta G_{rect})}, \tag{21}$$

we get the following numbers: r=4.4 for V_g=0 V and r=4.8 for V_g=[0,3.5] V. Rather than comparing the asymmetry at similar gate voltage, it would also be meaningful to compare them as a function of conductance, which gives r=1.7 for G=[4,10]e^2/h. Thus, $r>1$ in any interval and it can be concluded that the triangle is more asymmetric than the rectangle with regard to the induced net current in the nonlinear conductance.

It is interesting to note that the symmetric and antisymmetric parts of the net current are different for the triangle $T1$ and the rectangle R. Because $T1$ lacks LR symmetry, but is intentionally UD symmetric, we expect that the symmetric part is larger than the antisymmetric part for the triangle $T1$. However, for the rectangle, which is nominally both LR and UD symmetric, there is no reason for one being larger than the other. Indeed, for the triangle, the ratio between the standard deviation of the symmetric and antisymmetric parts is 2.0, while it is 1.2 for the rectangle, confirming the expectation.

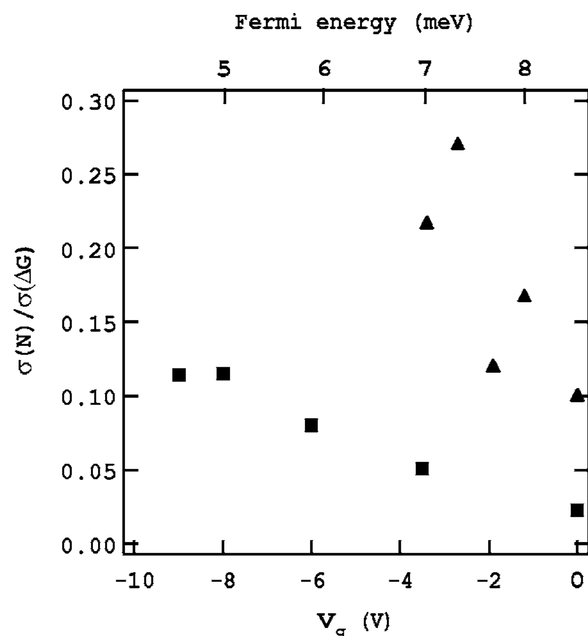

FIG. 12. The ratio of the standard deviation of the normalized net current and the conductance fluctuations $\sigma(N^{LR})/\sigma(\Delta G)$ is shown for the triangle $T1$ (triangles) and the rectangle R (squares) as a function of top gate voltage (Fermi energy) ($|B| \leq 100$ mT).

V. SUMMARY AND CONCLUSIONS

We have established symmetry relations for the nonlinear conductance of quantum dots with no, one, or two symmetry axes, taking into account the magnetic field and distinguishing nonrigid devices that show circuit-induced asymmetry and rigid devices that do not. All established symmetry relations are based on fundamental symmetry arguments and are expected to hold in the classical regimes as well as in the quantum regimes, regardless of the nature of the physical mechanism that causes the conduction asymmetry. Because it is *in praxis* not possible to fabricate a device that is perfectly symmetric on a microscopic scale, we experimentally investigated whether the expected symmetry relations can be observed in the regime of phase-coherent transport. One of the questions asked is, which of the expected symmetries, with respect to magnetic field direction, bias voltage, and grounding configuration, can indeed be observed? Another way of asking the same question is, how much geometric asymmetry is needed to generate rectification, and is the intended device geometry significant in comparison to unintended imperfections of the geometry?

Measurements of the nonlinear conductance in electron billiards that were defined by wet etching in InP/InGaAs material revealed all the symmetry relations expected for rigid devices of the given symmetry. Circuit-induced asymmetry was negligible in these devices. Although small deviations are observed as the result of imperfections, we conclude that the symmetry of the nonlinear conductance is indeed determined by the designed device geometry.

Using direct measurement of the rectified net current, we investigated the conductance symmetry in GaAs/AlGaAs devices. This measurement technique is much more sensitive to conductance asymmetries than a measurement of the conductance, because 100% of the measured signal is due to rectification. Using this technique, we find that the GaAs/AlGaAs devices show appreciable CIA effects, which we have shown how to remove from the data. The normalized net current $N(V,B)$ is not symmetric with respect to zero magnetic field for any of the UD-symmetric devices. However, for two of these devices ($T1$ and $T2$) we find a correlation between $N(B)$ and $N(-B)$ for low fields up to 20–50 mT and to larger fields in some cases. For C—a device without UD symmetry—there is no such correlation. These results show that our devices are not perfectly UD symmetric as measured by quantum-wave interference effects. However, there is a clear difference between devices that are intended to have UD symmetry and devices that are designed to lack UD symmetry. The importance of the device symmetry for the observed symmetry of nonlinear electron transport is underlined by the observation that the LR-symmetric device R induces much less net current than the triangle $T1$.

Some open questions remain. Let us start with the symmetry in B in the nonlinear response regime. It is known that generally $G(V,B) \neq G(V,-B)$ [Eq. (1)], while in the linear response regime the symmetry in B is almost perfect for any device of arbitrary shape.[1] Here (and in Ref. 20) we point out that this symmetry relation should be recovered for UD-symmetric devices—that is, $G(V,B)=G(V,-B)$. We also have a basic idea of the criteria which determine whether a device is measured in the linear response regime or in the nonlinear regime.[47] However, full qualitative and quantitative understanding of the magnitude of the asymmetry in Eq. (1) has not yet been established. Recently, Sánchez and Büttiker used random matrix theory to calculate the absolute magnitude of the expected conductance asymmetry in fully coherent quantum dots at $T=0$ as a function of the mode number in the contacts for the case of very small voltages ($V < E_T/e$, where the Thouless energy E_T is typically of the order of 10 μeV) and for magnetic flux smaller than Φ_0.[23] These results are consistent with work by Spivak and Zyuzin[27] on disordered systems and with recent experimental results on carbon nanotubes[24] and semiconductor quantum dots[26] for small flux and small bias voltage. Marlow *et al.*[25] recently measured the magnitude of the lowest-order nonlinear asymmetry in a magnetic field in phase-coherent electron billiards for $B \ll \Phi_0/A$ and for $V > E_T/e$. All of these authors find that the asymmetry in question is linear in B and V, but quantitative comparisons between the different experiments, and between experiment and theory, are currently difficult. More theoretical work is needed to tie together the small (B,V) regime with the results obtained for large B and V and to establish theoretical predictions that are applicable to dots at finite temperature and with limited phase-breaking times.

Another open question concerns the symmetry in B of the normalized net current $N(V_0,B)$ in the UD-symmetric triangle $T1$. Ideally, the antisymmetric part of $N(V_0,B)$ would equal zero for such a device, while the symmetric part would take finite values. What we observe indeed is that the antisymmetric part of the data is consistently smaller than the symmetric part. An observation that is not understood at present is that in Fig. 11 the frequency of the net current fluctuations appears to change at approximately 100 mT for the symmetric part, while this change is not equally significant for the antisymmetric part. Thus, the symmetric and antisymmetric parts of the fluctuations in B seem to have different frequencies as a function of B.

It is also not clear whether the same amount of geometric asymmetry is needed to induce a nonsymmetric nonlinear conductance in the phase-coherent regime compared to the noncoherent regime. One may imagine that only small deviations from a perfectly symmetric potential are needed in the phase-coherent regime, while it is not obvious that the same degree of deviation is sufficient to induce asymmetric conductance in the high-bias regime, where phase coherence is suppressed. If there is a difference, one would expect that for a UD-symmetric device the part that is antisymmetric in B would vanish at high bias. In Fig. 11 we show that the antisymmetric part does decrease slightly with increased bias voltage, but does not vanish entirely. Experiments addressing several of the open questions described above are currently in progress.

ACKNOWLEDGMENTS

We acknowledge Ivan Maximov for technical help and Hongqi Xu for helpful discussions. This project was supported by the Swedish Research Council, the Swedish Foundation for Strategic Research, the Australian Research Council, ONR, NSF CAREER Award No. PHY 0239764 (H.L.), NSF IGERT (C.A.M.), and a travel grant from the Swedish Institute (A.L.). R.P.T. acknowledges the support from the Research Corporation. The authors thank Claus B. Sørensen and the III-V NANOLAB of MIC and NBI for the MBE grown GaAs/AlGaAs material, and Werner Seifert for the InP/GaInAs material.

*Electronic address: anneli.lofgren@ftf.lth.se
†Electronic address: linke@uoregon.edu

[1] C. W. J. Beenakker and H. van Houten, in *Solid State Physics*, edited by H. Ehrenrich and D. Turnbull (Academic Press, New York, 1991), Vol. 44, p. 1.
[2] For a review see, e.g., J. P. Bird, J. Phys.: Condens. Matter **11**, R413 (1999).
[3] C. M. Marcus, A. J. Rimberg, R. M. Westervelt, P. F. Hopkins, and A. C. Gossard, Phys. Rev. Lett. **69**, 506 (1992); A. M. Chang, H. U. Baranger, L. N. Pfeiffer, and K. W. West, *ibid.* **73**, 2111 (1994); M. Persson, J. Pettersson, B. von Sydow, P. E. Lindelof, A. Kristensen, and K. F. Berggren, Phys. Rev. B **52**,

8921 (1995); K.-F. Berggren, Zhen-Li Ji, and Tomas Lundberg, *ibid.* **54**, 11612 (1996); J. P. Bird, D. K. Ferry, R. Akis, Y. Ochiai, K. Ishibashi, Y. Aoyagi, and T. Sugano, Europhys. Lett. **35**, 529 (1996); I. V. Zozoulenko, R. Schuster, K.-F. Berggren, and K. Ensslin, *ibid.* **55**, R10209 (1997); P. Bøggild, A. Kristensen, H. Bruus, S. M. Reimann, and P. E. Lindelof, *ibid.* **57**, 15408 (1998); I. V. Zozoulenko, A. S. Sachrajda, P. Zawadzki, K.-F. Berggren, Y. Feng, and Z. Wasilewski, *ibid.* **58**, 10597 (1998); T. Blomquist and I. V. Zozoulenko, *ibid.* **61**, 1724 (2000).

[4] H. Linke, L. Christensson, P. Omling, and P. E. Lindelof, Phys. Rev. B **56**, 1440 (1997).

[5] L. Christensson, H. Linke, P. Omling, P. E. Lindelof, I. V. Zozoulenko, and K.-F. Berggren Phys. Rev. B **57**, 12306 (1998).

[6] R. P. Taylor, A. S. Sachrajda, J. A. Adams, P. T. Coleridge, and P. Zawadzki, Phys. Rev. B **47**, 4458 (1993).

[7] R. P. Taylor, R. Newbury, A. S. Sachrajda, P. T. Coleridge, P. Zawadzki, R. B. Dunford, Y. Feng, J. P. Bird, C. R. Leavens, J. M. Cadogan, J. A. Adams, P. J. Kelly, M. Davies, and S. A. Brown, Semicond. Sci. Technol. **11**, 1189 (1996).

[8] V. I. Belinicher and B. I. Sturman, Usp. Fiz. Nauk **130**, 415 (1980) [Sov. Phys. Usp. **23**, 199 (1980)].

[9] A. Lorke, S. Wimmer, B. Jager, J. P. Kotthaus, W. Wegscheider, and M. Bichler, Physica B **251**, 312 (1998).

[10] A. M. Song, A. Lorke, A. Kriele, J. P. Kotthaus, W. Wegscheider, and M. Bichler, Phys. Rev. Lett. **80**, 3831 (1998).

[11] A. M. Song, Phys. Rev. B **59**, 9806 (1999).

[12] B. Hackens, L. Gence, C. Gustin, X. Wallart, S. Bollaert, A. Cappy, and V. Bayot, Appl. Phys. Lett. **85**, 4508 (2004).

[13] A. M. Song, P. Omling, L. Samuelson, W. Seifert, I. Shorubalko, and H. Zirath, Appl. Phys. Lett. **79**, 1357 (2001).

[14] H. Linke and A. M. Song, in *Electron Transport in Quantum Dots*, edited by J. P. Bird (Kluwer, Dordrecht, 2003).

[15] R. A. Webb, S. Washburn, and C. P. Umbach, Phys. Rev. B **37**, 8455 (1988).

[16] S. B. Kaplan, Surf. Sci. **196**, 93 (1988).

[17] P. A. M. Holweg, J. A. Kokkedee, J. Caro, A. H. Verbruggen, S. Radelaar, A. G. M. Jansen, and P. Wyder, Phys. Rev. Lett. **67**, 2549 (1991).

[18] D. C. Ralph, K. S. Ralls, and R. A. Buhrman, Phys. Rev. Lett. **70**, 986 (1993).

[19] R. Taboryski, A. K. Geim, M. Persson, and P. E. Lindelof, Phys. Rev. B **49**, R7813 (1994).

[20] H. Linke, W. D. Sheng, A. Svensson, A. Löfgren, L. Christensson, H. Q. Xu, P. Omling, and P. E. Lindelof, Phys. Rev. B **61**, 15914 (2000).

[21] H. Linke, W. D. Sheng, A. Löfgren, H. Q. Xu, P. Omling, and P. E. Lindelof, Europhys. Lett. **44**, 341 (1998).

[22] A. Löfgren, C. A. Marlow, I. Shorubalko, R. P. Taylor, P. Omling, L. Samuelson, and H. Linke, Phys. Rev. Lett. **92**, 046803 (2004).

[23] D. Sánchez and M. Büttiker, Phys. Rev. Lett. **93**, 106802 (2004).

[24] J. Wei, M. Shimogawa, Z. Wang, I. Radu, R. Dormaier, and D. H. Cobden, Phys. Rev. Lett. **95**, 256601 (2005).

[25] C. A. Marlow, R. P. Taylor, M. Fairbanks, I. Shorubalko, and H. Linke, Phys. Rev. Lett. **96**, 116801 (2006).

[26] D. M. Zumbühl, C. M. Marcus, M. P. Hanson, and A. C. Gossard, Phys. Rev. Lett. **96**, 206802 (2006).

[27] B. Spivak and A. Zyuzin, Phys. Rev. Lett. **93**, 226801 (2004).

[28] L. A. Ponomarenko, D. T. N. de Lang, A. de Visser, V. A. Kulbachinskii, G. Künzel, and A. M. M. Pruisken, Solid State Commun. **130**, 705 (2004).

[29] E. Peled, Y. Chen, E. Diez, D. C. Tsui, D. Shahar, D. L. Sivco, and A. Y. Cho, Phys. Rev. B **69**, 241305(R) (2004).

[30] B. Karmakar, M. R. Gokhale, A. P. Shah, B. M. Arora, D. T. N. de Lang, A. de Visser, L. A. Ponomarenko, and A. M. M. Pruisken, Physica E (Amsterdam) **24**, 187 (2004).

[31] S. Datta, *Electronic Transport in Mesoscopic Systems*, Vol 3 of *Cambridge Studies in Semiconductor Physics and Microelectronic Engineering* (Cambridge University Press, Cambridge, England, 1995).

[32] B. L. Al'tshuler and D. E. Khmel'nitskiĭ, Pis'ma Zh. Eksp. Teor. Fiz. **42**, 291 (1985) [Sov. Phys. JETP **42**, 359 (1985)].

[33] A. I. Larkin and D. E. Khmel'nitskiĭ, Zh. Eksp. Teor. Fiz. **91**, 1815 (1986) [Sov. Phys. JETP **64**], 1075 (1986); Phys. Scr. **T14**, 4 (1986).

[34] H. Linke, T. E. Humphrey, A. Löfgren, A. O. Sushkov, R. Newbury, R. P. Taylor, and P. Omling, Science **286**, 2314 (1999).

[35] M. Büttiker, Phys. Rev. Lett. **57**, 1761 (1986).

[36] M. Büttiker, IBM J. Res. Dev. **32**, 317 (1988).

[37] L. P. Kouwenhoven, B. J. van Wees, C. J. P. M. Harmans, J. G. Williamson, H. van Houten, C. W. J. Beenakker, C. T. Foxon, and J. J. Harris, Phys. Rev. B **39**, 8040 (1989).

[38] L. Martín-Moreno, J. T. Nicholls, N. K. Patel, and M. Pepper, J. Phys.: Condens. Matter **4**, 1323 (1992).

[39] A. Kristensen, H. Bruus, A. E. Hansen, J. B. Jensen, P. E. Lindelof, C. J. Marckmann, J. Nygård, S. B. Sørensen, F. Beuscher, A. Forchel, and M. Michel, Phys. Rev. B **62**, 10950 (2000).

[40] Another way of avoiding this contribution is to set the reference point of the gate to half of the applied bias. This approach was not employed because it introduced significant noise in the measurements.

[41] P. Ramvall, N. Carlsson, P. Omling, L. Samuelson, W. Seifert, M. Stolze, and Q. Wang, Appl. Phys. Lett. **68**, 1111 (1996).

[42] I. Maximov, Q. Wang, M. Graczyk, P. Omling, L. Samuelson, W. Seifert, and I. Shorubalko, in *Proceedings of 11th Internattional Conference on InP and Related Materials*, Davos, 1999 (Institute of Electrical and Electronics Engineers, Davos, Switzerland, 1999), p. 237.

[43] T. P. Martin, R. P. Taylor, H. Linke, C. A. Marlow, G. D. R. Hall, I. Shorubalko, I. Maximov, W. Seifert, L. Samuelson, and T. M. Fromhold, Superlattices Microstruct. **34**, 179 (2003).

[44] A. Löfgren, Ph.D. thesis, Lund University, 2002.

[45] T. E. Humphrey, Ph.D. thesis, University of New South Wales, Sydney, Australia, 2003.

[46] H. Linke, J. P. Bird, J. Cooper, P. Omling, Y. Aoyagi, and T. Sugano, Phys. Rev. B **56**, 14937 (1997).

[47] H. Linke, H. Q. Xu, A. Löfgren, W. D. Sheng, A. Svensson, P. Omling, P. E. Lindelof, R. Newbury, and R. P. Taylor, Physica B **272**, 61 (1999).

[48] M. Switkes, A. G. Huibers, C. M. Marcus, K. Campman, and A. C. Gossard, Appl. Phys. Lett. **72**, 471 (1998).